

Metal-tuned W₁₈O₄₉ for efficient electrocatalytic N₂ reduction

Mengmeng Yang,^a Rupeng Huo,^a Huidong Shen,^a Qineng Xia,^{*b} Jieshan Qiu,^c Alex W. Robertson,^d Xi Li^b and Zhenyu Sun^{*a}

^a State Key Laboratory of Organic-Inorganic Composites, Beijing University of Chemical Technology, Beijing 100029, P. R. China.

^b College of Biological, Chemical Science and Engineering, Jiaxing University, Jiaxing 314001, Zhejiang, P. R. China.

^c State Key Laboratory of Chemical Resource Engineering, Beijing University of Chemical Technology, Beijing 100029, P. R. China.

^d Department of Materials, University of Oxford, Oxford OX1 3PH, UK.

ABSTRACT: Electrochemical N₂ reduction (ENR) offers a promising route for NH₃ production. To promote this kinetically sluggish process, the design and development of electrocatalysts with high performance, good durability, low cost, and earth abundance are highly demanded. Here we report a facile strategy for the synthesis of metal-doped ultrafine W₁₈O₄₉ nanowires with significantly enhanced capability for electrocatalytic N₂ reduction to produce NH₃ in a wide pH range. In particular, the Mo-doped W₁₈O₄₉ catalyst can convert N₂ to NH₃ with a faradaic efficiency approaching 12.1% at −0.2 V (versus the reversible hydrogen electrode, vs. RHE) and an NH₃ yield rate of 5.3 μg h^{−1} mg_{cat.}^{−1} at −0.5 V (vs. RHE) in 0.1 M Na₂SO₄, which is about two times higher than pristine W₁₈O₄₉. We find occurrence of strong electron transfer from Mo to W, which facilitates N₂ adsorption and activation, thus accelerating the ENR to generate NH₃. This work provides a simple and effective method to modify metal oxides for efficient electrochemical N₂ fixation.

KEYWORDS: *N₂ reduction, electrocatalysis, doping, metal oxide*

INTRODUCTION

NH₃ is an indispensable chemical in modern life, which is widely utilized in agriculture, medicine, textile, and many other industries.¹ NH₃ can also be used as a stable hydrogen carrier due to its liquefiability and carbon-free feature.² Up to now, the Haber-Bosch process is still the main method to synthesize ammonia in industry. However, this process has intrinsic drawbacks such as high-energy consumption, requirements of sophisticated facilities and running cost, and large amounts of CO₂ emissions.³ Therefore, there are now intensive efforts to attain NH₃ synthesis through green routes under ambient conditions.⁴⁻⁶

Electrochemical N₂ reduction (ENR) powered by renewable electricity provides an environmentally friendly and sustainable way for ammonia synthesis.⁷⁻¹¹ However, N₂ is a thermodynamically stable and kinetically inert molecule with strong N≡N bond (940.1 kJ mol^{−1}) and low polarizability. Binding and activation of N₂ in mild conditions are challenging.⁵ So far, a variety of electrocatalysts including transition metal-based materials (Au,¹² Pt,¹³ Ru,¹⁴ Rh,¹⁵ Pd,¹⁶ Cu,¹⁷ Fe,¹⁸ Bi₄V₂O₁₁/CeO₂,¹⁹ and TiO₂²⁰) and non-metallic catalysts (N-doped porous carbon,²¹⁻²²

defective reduced graphene oxide,²³ doped few-layer graphene,²⁴ black phosphorus,²⁵ and boron²⁶⁻²⁷) have been demonstrated to enable N₂ reduction. Despite these recent advances, the design and development of efficient and stable catalyst for ENR remains an ongoing challenge.

Tungsten oxide-based materials have recently received great attention as both photocatalysts and electrocatalysts for N₂ fixation.²⁸⁻³⁰ Oxygen-vacancy rich tungsten trioxide (WO_{3-x}) has been reported to increase N₂ adsorption, facilitate N₂ activation, and lower NRR thermodynamic overpotentials.²⁹⁻³⁰ W₁₈O₄₉ nanowires (NWs) with anisotropic growth along the direction of [010], have abundant surface oxygen vacancies,³¹ showing a great potential in catalysis. However, W₁₈O₄₉ NWs with tailored surface vacancies have not been explored for electrocatalytic nitrogen fixation to date.

In this work, we report for the first time facile doping of ultrafine W₁₈O₄₉ NWs with various metals (Mn, Sb, Y, Fe, Sn, Pd, and Mo) for enhanced ENR to produce NH₃. Among these dopants, Mo shows the best capability to boost the ENR activity of W₁₈O₄₉, enabling an NH₃ faradaic efficiency (FE) exceeding 12.0% at -0.2 V (versus reversible hydrogen electrode, *vs.* RHE) and NH₃ yield rate of about 5.3 μg h⁻¹ mg_{cat.}⁻¹ at -0.5 V (*vs.* RHE) in neutral electrolyte, significantly outperforming undoped W₁₈O₄₉. All potentials used in this work are reference to RHE.

RESULTS AND DISCUSSION

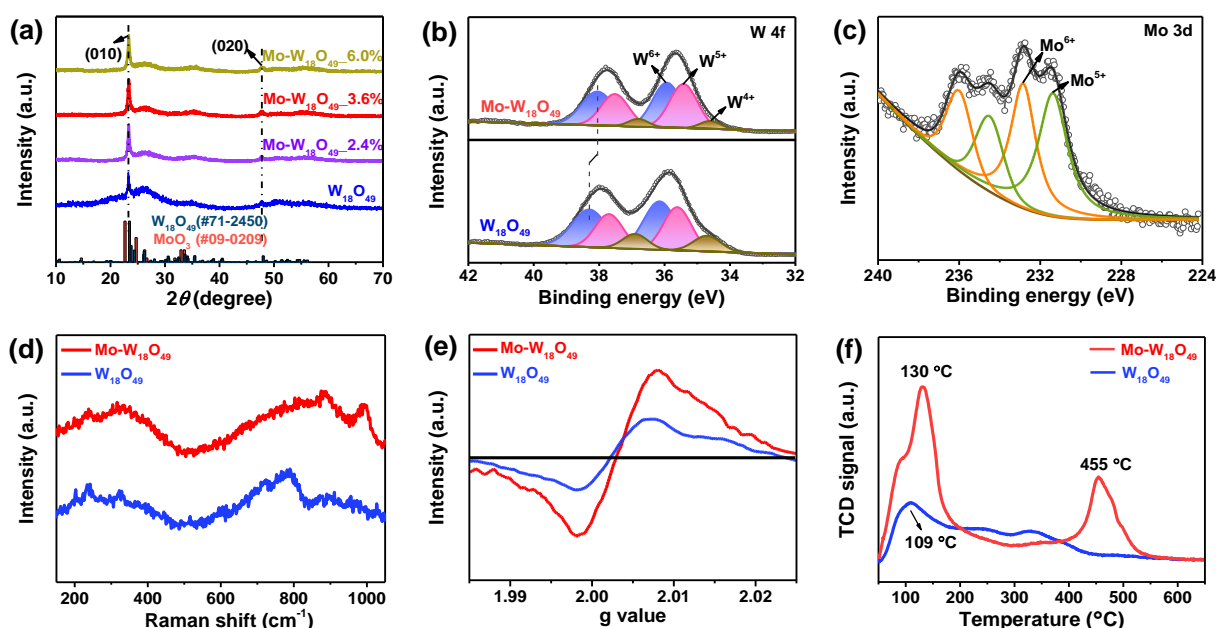


Figure 1. (a) XRD patterns of W₁₈O₄₉ and Mo-W₁₈O₄₉ with different Mo doping contents. (b) W 4f XPS spectra of W₁₈O₄₉ and Mo-W₁₈O₄₉. (c) Mo 3d XPS of Mo-W₁₈O₄₉. (d) Raman spectra, (e) ESR spectra, and (f) N₂-TPD results of W₁₈O₄₉ and Mo-W₁₈O₄₉. The Mo doping content in the Mo-W₁₈O₄₉ shown in b-f is 3.6 wt%.

Here, we synthesize doped W₁₈O₄₉ ultrafine NWs with a variety of metals such as Mn, Sb, Y, Fe, Sn, Pd, and Mo via a very simple solvothermal process. The contents of Mo in the doped catalyst were determined by inductively coupled plasma-atomic emission spectrometry (ICP-AES), the

results of which are consistent with theoretical calculations. The X-ray diffraction (XRD) patterns of the Mo-doped $W_{18}O_{49}$ (Mo- $W_{18}O_{49}$) samples with different doping levels are given in Fig. 1a. The diffraction peaks at 23.3 and 47.7° can be well assigned to the (010) and (020) planes of monoclinic $W_{18}O_{49}$ (JCPDS No.71-2450) in all cases.³² The (010) reflection is slightly shifted toward higher 2θ after Mo doping, which may be caused by lattice mismatch upon surface decoration or by the presence of interstitial heteroatoms.³³

X-ray photoelectron spectroscopy (XPS) was used to detect surface composition and chemical state of Mo- $W_{18}O_{49}$ (Fig. S1 and Fig. 1b and c). Shown in Fig. 1b are the W 4f XPS spectra of Mo- $W_{18}O_{49}$, which manifest a strong doublet with binding energies (BEs) at 35.9 and 38.0 eV attributed to W^{6+} and also two doublet peaks with BEs at 35.4 and 37.5 eV assigned to W^{5+} , and BEs at 34.6 and 36.8 eV corresponding to W^{4+} .²⁹ Note that all the W 4f peaks are shifted significantly to lower BEs after Mo doping, indicating transfer of electrons from Mo to W. As displayed in Fig. 1c, two doublet peaks can be seen with Mo $3d_{5/2}$ at 231.3 and 232.8 eV and Mo $3d_{3/2}$ at 234.5 and 236.1 eV, corresponding to Mo^{5+} and Mo^{6+} .^{29, 32} The presence of high-valence Mo species (Mo^{6+}) is likely associated with electron transfer from Mo to W. An apparent O 1s XPS peak at 532.3 eV originating from adsorbed oxygen species largely retained (Fig. S1b), which suggests the preservation of abundant oxygen defects after Mo doping.⁶

Raman spectra exhibit the typical bending vibrations of O–W–O at *ca.* 236 and 323 cm^{-1} as well as stretching modes of O–W–O at *ca.* 723 and 790 cm^{-1} , and a weak stretching mode of the terminal W=O at *ca.* 962 cm^{-1} in Mo- $W_{18}O_{49}$ (Fig. 1d).³⁰ The peaks are broader than those of unmodified $W_{18}O_{49}$ and the intensities of the shoulder peaks around 750 to 850 cm^{-1} are enhanced likely due to the shorter length of the Mo–O bonds generated during Mo doping.³⁵ The band at *ca.* 991 cm^{-1} can be ascribed to the stretching mode of Mo=O.³⁵

Electron spin resonance (ESR) spectra show a pair of peaks with a symmetric distribution (Fig. 1e) for both $W_{18}O_{49}$ and Mo- $W_{18}O_{49}$ in accordance with a signal at $g \approx 2.007$ for free electrons, an indication of rich oxygen vacancies in the samples. These peaks are enhanced after Mo doping. This suggests creation of more unpaired electrons, which delocalize over the lattice of $W_{18}O_{49}$, beneficial to electron transfer to adsorbates during the ENR process.

N_2 temperature-programmed desorption (TPD) profiles display substantially enhanced N_2 adsorption after Mo doping of $W_{18}O_{49}$ (Fig. 1f). Two desorption peaks centered at 130 and 455 °C over Mo- $W_{18}O_{49}$ can be attributed to N_2 physisorption and N_2 chemisorption, respectively. In stark contrast to pristine $W_{18}O_{49}$, both desorption peaks of Mo- $W_{18}O_{49}$ are shifted to higher temperatures, illustrating strengthened N_2 adsorption in favour of ENR.

The composition, morphology, and microstructure of the Mo- $W_{18}O_{49}$ were further examined by transmission electron microscopy (TEM) (Figs. 2 and S2). The sample predominantly exhibits one-dimensional (1D) nanostructures with length on a micrometre scale, and no other dimensional morphologies were observed. High-angle annular dark-field scanning transmission electron microscopy (HAADF-STEM) (Fig. 2a) along with energy dispersive X-ray spectroscopy (EDS) spectrum (Fig. 2b) and elemental maps (Fig. 2c-e) confirms that the NWs are composed of W, O,

and Mo, indicating successful Mo doping of $W_{18}O_{49}$. High-resolution TEM (HRTEM) observation reveals the formation of ultrathin crystalline NWs with a diameter of less than 5 nm (Fig. 2f, g, and i). The large ratio of length to diameter provides high surface areas to expose more active sites, which may favor high catalytic activity. Many NWs are oriented parallel to each other forming bundles, probably due to van der Waals forces between neighbouring NWs (Fig. 2f). As observed by HRTEM (Fig. 2g and i) in combination with Fast Fourier transform (FFT) (Fig. 2h and j), the ordered lattice fringes with a spacing of about 3.7 Å are ascribed to the (010) planes, suggesting that the NWs grow along the [010] direction.

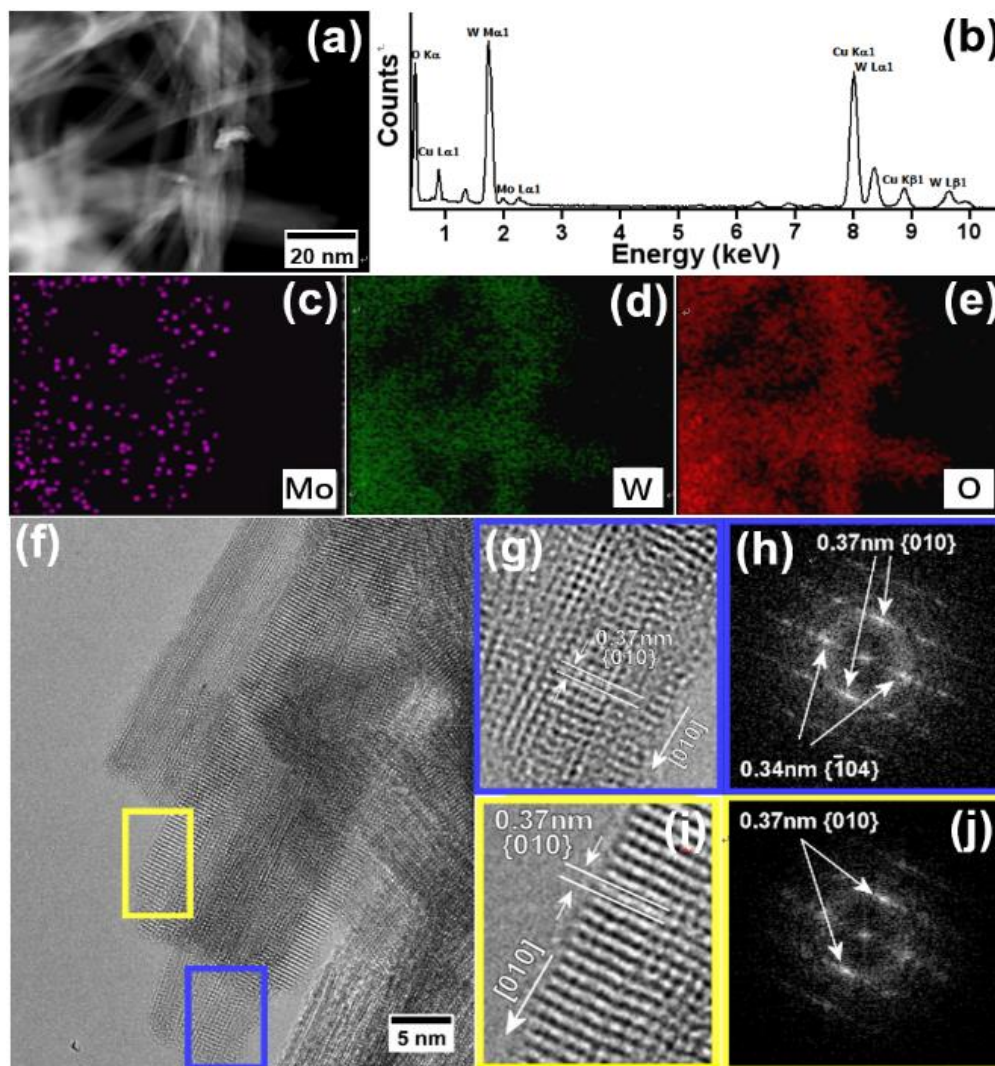


Figure 2. (a) HAADF-STEM image of Mo- $W_{18}O_{49}$. EDS spectrum (b) and elemental maps of (c) O, (d) Mo, and (e) W. (f) HRTEM image of Mo- $W_{18}O_{49}$. (g)-(j) correspond to magnified images and corresponding FFTs of the regions enclosed by the yellow and blue rectangles in f.

The Mo- $W_{18}O_{49}$ catalysts were evaluated for ENR using a carbon paper working electrode in an H-type cell separated by a Nafion 117 membrane under ambient conditions. Shown in Fig. 3a are the linear sweep voltammetry (LSV) curves of Mo- $W_{18}O_{49}$ and $W_{18}O_{49}$ in Ar- and N_2 -saturated 0.1 M Na_2SO_4 solution. The current densities in the N_2 -saturated electrolyte are higher than in the Ar-

saturated one in both cases, indicating occurrence of N_2 reduction. Strikingly, $Mo-W_{18}O_{49}$ exhibits remarkably enhanced current densities compared to pristine $W_{18}O_{49}$ in N_2 -saturated electrolyte. This indicates that Mo doping of $W_{18}O_{49}$ can accelerate ENR. ENR occurs at potentials ≥ -0.2 V with an overpotential of ≤ 0.206 V (given the thermodynamic potential for N_2 reduction to NH_3 is 0.06 V vs. normal hydrogen electrode under our experimental conditions (298 K and 1 atm)) when using Mo-

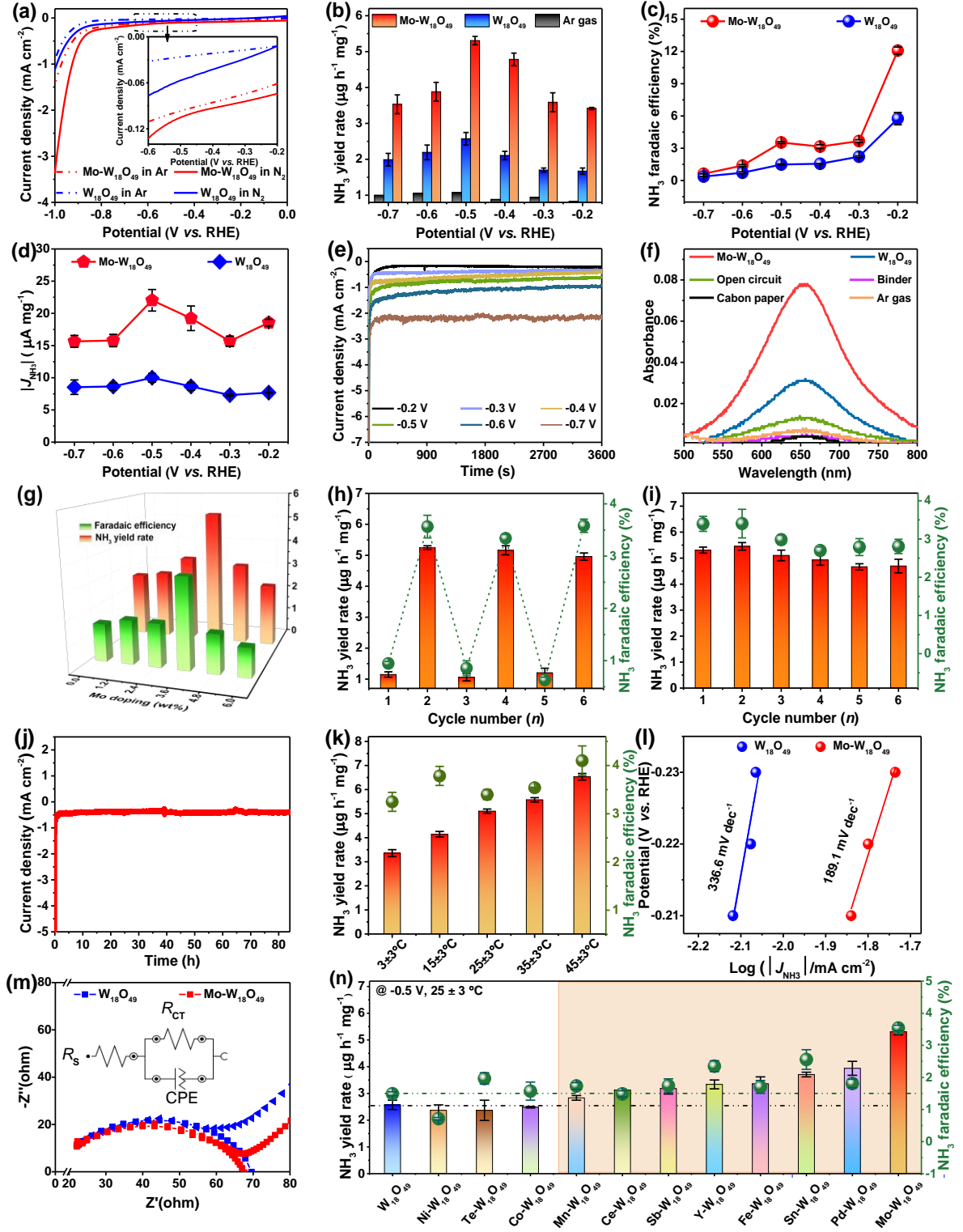


Figure 3. (a) The LSV results of $W_{18}O_{49}$ and Mo- $W_{18}O_{49}$ on glassy carbon electrode in Ar- (dashed line) or N_2 (solid line)-saturated 0.1 M aqueous Na_2SO_4 with a scan rate of 5 mV s^{-1} . (b) The NH_3 yield rate against applied potential over $W_{18}O_{49}$ and Mo- $W_{18}O_{49}$ in N_2 -saturated 0.1 M Na_2SO_4 solution as well as in Ar-saturated 0.1 M Na_2SO_4 solution over Mo- $W_{18}O_{49}$. (c) and (d) The NH_3 FEs and NH_3 partial current densities at different applied potentials over $W_{18}O_{49}$ and Mo- $W_{18}O_{49}$. (e) Chronoamperometric curves of Mo- $W_{18}O_{49}$ at various potentials. (f) UV-vis absorption spectra of the electrolytes after electrolysis at -0.5 V for the control experiments with Ar-saturated electrolyte (Ar gas), or without the Mo- $W_{18}O_{49}$ catalyst (Carbon paper), or with only the background Nafion solution (Binder), or at an open circuit (Open circuit). (g) The FE and yield rate for NH_3 formation as a function of Mo doping content over Mo- $W_{18}O_{49}$. (h) The FE and yield rate for NH_3 formation over Mo- $W_{18}O_{49}$ with alternated cycles between Ar- and N_2 -saturated 0.1 M Na_2SO_4 at -0.5 V . (i) Long-term durability and (j) chronoamperometry measurements at -0.5 V over Mo- $W_{18}O_{49}$ electrode. (k) Electrolysis temperature effect on FE and yield rate of NH_3 over Mo- $W_{18}O_{49}$. (l) Tafel plots and (m) electrochemical impedance spectroscopy (EIS) profiles of $W_{18}O_{49}$ and Mo- $W_{18}O_{49}$. (n) The FEs and yield rates of NH_3 over $W_{18}O_{49}$ and various metal-doped $W_{18}O_{49}$ at -0.5 V . The electrolytes used in c, d, e, g, h, i, j, m, and n are N_2 -saturated 0.1 M Na_2SO_4 solution. The metal doping level in all the modified $W_{18}O_{49}$ catalysts is 3.6 wt%.

$W_{18}O_{49}$ as a cathode catalyst (Fig. 3b-d). The total current density increased steadily from -0.2 to -2.1 mA cm^{-2} when the potential shifted from -0.2 to -0.7 V (Fig. 3e). Only NH_4^+ was detected by the indophenol blue method in our system (Fig. S3). No N_2H_4 was identified by the Watt and Chrisp method³⁶ within the detection limit of the approach. The NH_3 yield rate of Mo- $W_{18}O_{49}$ was observed to initially increase from -0.2 to -0.5 V and then drop with further increase of applied potential, likely associated with occurrence of enhanced parasitic HER at more negative potentials.³⁰ The maximum NH_3 yield rate reaches *ca.* $5.3\text{ }\mu\text{g h}^{-1}\text{ mg}_{\text{cat}}^{-1}$ at -0.5 V , in contrast to that of *ca.* $2.6\text{ }\mu\text{g h}^{-1}\text{ mg}_{\text{cat}}^{-1}$ for $W_{18}O_{49}$ (Fig. 3b). The NH_3 FE for Mo- $W_{18}O_{49}$ is 12.1%, over twice as high as that of 5.8% for pristine $W_{18}O_{49}$ at -0.2 V (Fig. 3c). Similarly, the NH_3 partial current is *ca.* $22.0\text{ }\mu\text{A cm}^{-2}$, one time higher than that of $W_{18}O_{49}$. These results verify that Mo doping significantly improved the ENR activity of $W_{18}O_{49}$.

To confirm the origin of the evolved NH_3 , we carried out multiple control and blank experiments. Very little or no NH_3 was generated in argon (99.999% purity)-saturated 0.1 M Na_2SO_4 (Ar gas), or with carbon paper electrode in the absence of Mo- $W_{18}O_{49}$ (Carbon paper), or with only the background Nafion solution binder (Binder), or at an open circuit as a control (Open circuit), as presented in Fig. 3f. The influence of possible contamination from the air can be ruled out by the result that negligible NH_4^+ was detected after leaving the electrolytes in air for different periods (Fig. S4).

The effect of Mo doping level was investigated for ENR in terms of both FE and yield rate for NH_3 formation. The optimal Mo doping content was found to be 3.6 wt%, as illustrated in Fig. 3g. The impact of catalyst synthesis temperature was also studied, the results of which showed the highest ENR catalytic activity at $210\text{ }^\circ\text{C}$ (Fig. S5). Alternating electrolysis cycle measurements between Ar and N_2 -saturated electrolytes indicated that the NH_3 generated exclusively originated

from the feed gas N_2 and could remain nearly constant for 6 cycles (Fig. 3h). Additionally, cycling test in N_2 -saturated electrolytes showed rather good stability of the Mo- $W_{18}O_{49}$ catalyst with NH_3 yield rate of about $4.7 \mu g \cdot h^{-1} mg^{-1}$ at $-0.5 V$ even after six cycles (Fig. 3i). Further, chronoamperometry measurements show that after 84 hours, the overall current density is essentially constant (Fig. 3j). The NH_3 yield rate was found to increase correspondingly with the ENR temperature (Fig. 3k). This is likely due to enhanced mass transport at elevated temperatures, thus accelerating N_2 reduction. The NH_3 yield rate approaches $6.5 \mu g h^{-1} mg_{cat.}^{-1}$ at $45 \pm 3 ^\circ C$. We also studied the ENR over Mo- $W_{18}O_{49}$ and $W_{18}O_{49}$ under alkaline (0.1 M KOH) and acidic (0.1 M HCl) conditions (Figs. S6 and S7). Even though a smaller NH_3 yield rate and NH_3 FE were obtained in these electrolytes compared to the neutral electrolyte, Mo- $W_{18}O_{49}$ still remarkably exceeds $W_{18}O_{49}$ in all the cases, confirming the critical role of Mo doping for enhanced ENR. To further explain the superior activity of Mo- $W_{18}O_{49}$, the Tafel plot and electrochemical impedance were investigated. The Tafel slope, an indication of the kinetics for NH_3 evolution, is $\sim 189.1 mV dec^{-1}$ for Mo- $W_{18}O_{49}$ (Fig. 3l), substantially lower than that of $\sim 336.6 mV dec^{-1}$ for $W_{18}O_{49}$. This suggests that Mo doping greatly promotes N_2 reduction kinetics and the formation of $*N_2H$ (the first electron-transfer step, * represents the surface-adsorbed species) determines the reaction rate.²³ Nyquist plots (Fig. 3m) display that the Mo- $W_{18}O_{49}$ catalyst facilitates a slightly more rapid interfacial charge transfer between the catalyst film and reactants in the electrolyte compared to $W_{18}O_{49}$, matching with its observed higher ECR activity.

Interestingly, we also identified several other metals such as Mn, Sb, Y, Fe, Sn, and Pd, which boost ENR over $W_{18}O_{49}$ upon doping with these metals (Fig. 3n). Further work on optimization of ENR performance and exploration of doping effects in these systems is under way.

CONCLUSIONS

In summary, we have demonstrated remarkable enhancement of $W_{18}O_{49}$ nanowires for ENR via doping with a variety of metals. The as-obtained Mo-doped $W_{18}O_{49}$ can catalyze ENR in a wide pH range, providing an NH_3 FE of up to about 12.1% at $-0.2 V$ and an NH_3 yield rate of about $5.3 \mu g h^{-1} mg_{cat.}^{-1}$ at $\sim 25 ^\circ C$ ($6.5 \mu g h^{-1} mg_{cat.}^{-1}$ at $\sim 45 ^\circ C$) in 0.1 M Na_2SO_4 solution, over twice as high as that of unmodified $W_{18}O_{49}$ under similar conditions. Pronounced electron transfer from Mo to W occurs, which facilitates N_2 adsorption and activation, thus promoting the ENR to produce NH_3 . This work provides a potential route to modify metal oxides for efficient electrochemical N_2 fixation.

ASSOCIATED CONTENT

Supporting Information

The Supporting Information is available free of charge on the ACS Publications website.

Experimental details; EDX spectrum; XPS spectra of $W_{18}O_{49}$ and Mo- $W_{18}O_{49}$; The NH_3 yield rate and FE over Mo-doped $W_{18}O_{49}$ obtained at different temperatures; The NH_3 yield rate and FE over Mo- $W_{18}O_{49}$ and $W_{18}O_{49}$ under alkaline (0.1 M KOH) and acidic (0.1 M HCl) conditions.

AUTHOR INFORMATION

Corresponding Authors

*(Z.S.) E-mail: sunzy@mail.buct.edu.cn.

*(Q.X.) E-mail: xiaqineng@mail.zjxu.edu.cn.

Author Contributions

M.Y. designed and conducted the experiments. S. wrote the paper and supervised the project. A.R. performed STEM characterization. All authors contributed to discussions and revisions of the paper.

Notes

There is no competing financial interest to declare.

ACKNOWLEDGMENTS

This work was supported by National Natural Science Foundation of China (NSFC, No. 21972010); Beijing Natural Science Foundation (No. 2192039); the State Key Laboratory of Organic-Inorganic Composites (No. oic-201901001); and Beijing University of Chemical Technology (XK180301). A.W.R. acknowledges support from EPSRC South of England Analytical Electron Microscopy EP/K040375/1.

REFERENCES

- (1) Andersen, S. Z.; Čolić, V.; Yang, S.; Schwalbe, J. A.; Nielander, A. C.; McEnaney, J. M.; Enemark-Rasmussen, K.; Baker, J. G.; Singh, A. R.; Rohr, B. A.; Statt M. J.; Blair, S. J.; Mezzavilla, S.; Kibsgaard, J.; Vesborg, P. C. K.; Cargnello, M.; Bent, S. F.; Jaramillo, T. F.; Stephens, I. E. L.; Kørskov, J. K.; Chorkendorff, I. A rigorous electrochemical ammonia synthesis protocol with quantitative isotope measurements. *Nature* **2019**, 570, 504–508, DOI 10.1038/s41586-019-1625-1.
- (2) Guo, J.; Chen, P. Catalyst: NH_3 as an energy carrier. *Chem* **2017**, 3 (5), 709-712, DOI 10.1016/j.chempr.2017.10.004.
- (3) Honkala, K.; Hellman, A.; Remediakis, I.; Logadottir, A.; Carlsson, A.; Dahl, S.; Christensen, C. H.; Nørskov, J. K. Ammonia synthesis from first-principles calculations. *Science* **2005**, 307 (5709), 555-558, DOI 10.1126/science.1106435.
- (4) Chen, J. G.; Crooks, R. M.; Seefeldt, L. C.; Bren, K. L.; Bullock, R. M.; Darensbourg, M. Y.; Holland, P. L.; Hoffman, B.; Janik, M. J.; Jones, A. K. Beyond fossil fuel-driven nitrogen transformations. *Science* **2018**, 360 (6391), eaar6611, DOI 10.1126/science.aar6611.
- (5) Guo, C.; Ran, J.; Vasileff, A.; Qiao, S.-Z. Rational design of electrocatalysts and photo (electro) catalysts for nitrogen reduction to ammonia (NH_3) under ambient conditions. *Energy Environ. Sci.* **2018**, 11 (1), 45-56, DOI 10.1039/C7EE02220D.
- (6) Ying, Z.; Chen, S.; Zhang, S.; Peng, T.; Li, R. Efficiently enhanced N_2 photofixation performance of sea-urchin-like $\text{W}_{18}\text{O}_{49}$ microspheres with Mn-doping. *Appl. Catal. B Environ.* **2019**, 254, 351-359, DOI 10.1016/j.apcatb.2019.05.005.
- (7) Liu, K.-H.; Zhong, H.-X.; Li, S.-J.; Duan, Y.-X.; Shi, M.-M.; Zhang, X.-B.; Yan, J.-M.; Jiang, Q. Advanced catalysts for sustainable hydrogen generation and storage via hydrogen evolution and carbon dioxide/nitrogen

- reduction reactions. *Prog. Mater. Sci.* **2018**, 92, 64-111, DOI 10.1016/j.pmatsci.2017.09.001.
- (8) Cui, X.; Tang, C.; Zhang, Q. A review of electrocatalytic reduction of dinitrogen to ammonia under ambient conditions. *Adv. Energy Mater.* **2018**, 8 (22), 1800369, DOI 10.1002/aenm.201800369.
- (9) Zhang, L.; Chen, G.-F.; Ding, L.-X.; Wang, H. H. Advanced non-metallic catalysts for electrochemical nitrogen reduction under ambient conditions. *Chem. Eur. J.* **2019**, 25, 12464-12485, DOI 10.1002/chem.201901668.
- (10) Tang, C.; Qiao, S.-Z. How to explore ambient electrocatalytic nitrogen reduction reliably and insightfully. *Chem. Soc. Rev.* **2019**, 48, 3166-3180, DOI 10.1039/C9CS00280D.
- (11) Cheng, H.; Cui, P.; Wang, F.; Ding, L. X.; Wang, H. H. High efficiency electrochemical nitrogen fixation achieved with a lower pressure reaction system by changing the chemical equilibrium. *Angew. Chem. Int. Ed.* **2019**, 58 (43), 15541-15547. DOI 10.1002/anie.201910658.
- (12) Li, Y.; Zheng, J.; Lyu, Y.; Qiao, M.; Veder, J. P.; Marco, R. D.; Bradley, J.; Wang, R.; Huang, A.; Wang, S. Electron localization of gold in control of nitrogen-to-ammonia fixation. *Angew. Chem. Int. Ed.* **2019**, 58, 2-8, DOI 10.1002/anie.201909477.
- (13) Yao, Y.; Zhu, S.; Wang, H.; Li, H.; Shao, M. A spectroscopic study on the nitrogen electrochemical reduction reaction on gold and platinum surfaces. *J. Am. Chem. Soc.* **2018**, 140 (4), 1496-1501, DOI 10.1021/jacs.7b12101.
- (14) Tao, H.; Choi, C.; Ding, L.-X.; Jiang, Z.; Han, Z.; Jia, M.; Fan, Q.; Gao, Y.; Wang, H.; Robertson, A. W.; Hong, S.; Jung, Y.; Liu, S.; Sun, Z. Nitrogen fixation by Ru single-atom electrocatalytic reduction. *Chem.* **2019**, 5 (1), 204-214, DOI 10.1016/j.chempr.2018.10.007.
- (15) Liu, H.-M.; Han, S.-H.; Zhao, Y.; Zhu, Y.-Y.; Tian, X.-L.; Zeng, J.-H.; Jiang, J.-X.; Xia, B. Y.; Chen, Y. Surfactant-free atomically ultrathin rhodium nanosheet nanoassemblies for efficient nitrogen electroreduction. *J. Mater. Chem. A* **2018**, 6 (7), 3211-3217, DOI 10.1039/C7TA10866D.
- (16) Wang, J.; Yu, L.; Hu, L.; Chen, G.; Xin, H.; Feng, X. Ambient ammonia synthesis via palladium-catalyzed electrohydrogenation of dinitrogen at low overpotential. *Nat. Commun.* **2018**, 9 (1), 1795, DOI 10.1038/s41467-018-04213-9.
- (17) Lin, Y. X.; Zhang, S. N.; Xue, Z. H.; Zhang, J. J.; Su, H.; Zhao, T. J.; Zhai, G. Y.; Li, X. H.; Antonietti, M.; Chen, J. S. Boosting selective nitrogen reduction to ammonia on electron-deficient copper nanoparticles. *Nat. Commun.* **2019**, 10 (1), 1-7, DOI 10.1038/s41467-019-12312-4.
- (18) Chen, S.; Perathoner, S.; Ampelli, C.; Mebrahtu, C.; Su, D.; Centi, G. Electrocatalytic synthesis of ammonia at room temperature and atmospheric pressure from water and nitrogen on a carbon - nanotube - based electrocatalyst. *Angew. Chem. Int. Ed.* **2017**, 56 (10), 2699-2703, DOI 10.1002/anie.201609533.
- (19) Lv, C.; Yan, C.; Chen, G.; Ding, Y.; Sun, J.; Zhou, Y.; Yu, G. An amorphous noble - metal - free electrocatalyst that enables nitrogen fixation under ambient conditions. *Angew. Chem. Int. Ed.* **2018**, 57 (21), 6073-6076, DOI 10.1002/anie.201801538.
- (20) Han, Z.; Choi, C.; Hong, S.; Wu, T.-S.; Soo, Y.-L.; Jung, Y.; Qiu, J.; Sun, Z. Activated TiO₂ with tuned vacancy for efficient electrochemical nitrogen reduction. *Appl. Catal. B: Environ.* **2019**, 257, 117896, DOI 10.1016/j.apcatb.2019.117896.
- (21) Liu, Y.; Su, Y.; Quan, X.; Fan, X.; Chen, S.; Yu, H.; Zhao, H.; Zhang, Y.; Zhao, J. Facile ammonia synthesis from electrocatalytic N₂ reduction under ambient conditions on N-doped porous carbon. *ACS Catal.* **2018**, 8 (2), 1186-1191, DOI 10.1021/acscatal.7b02165.
- (22) Mukherjee, S.; Cullen, D. A.; Karakalos, S.; Liu, K.; Zhang, H.; Zhao, S.; Xu, H.; More, K. L.; Wang, G.; Wu, G. Metal-organic framework-derived nitrogen-doped highly disordered carbon for electrochemical ammonia synthesis using N₂ and H₂O in alkaline electrolytes. *Nano Energy* **2018**, 48, 217-226, DOI 10.1016/j.nanoen.2018.03.059.
- (23) Zhang, M. L.; Choi, C.; Huo, R. P.; Gu, G. H.; Hong, S.; Yan, C.; Xu, S. Y.; Robertson, A. W.; Qiu, J. S.; Jung,

- Y. ; Sun, Z. Y. Reduced graphene oxides with engineered defects enable efficient electrochemical reduction of dinitrogen to ammonia in wide pH range. *Nano Energy* **2020**, 68, 104323, DOI 10.1016/j.nanoen.2019.104323
- (24) Yu, X.; Han, P.; Wei, Z.; Huang, L.; Gu, Z.; Peng, S.; Ma, J.; Zheng, G. Boron-doped graphene for electrocatalytic N₂ reduction. *Joule* **2018**, 2 (8), 1610-1622, DOI 10.1016/j.joule.2018.06.007.
- (25) Zhang, L.; Ding, L. X.; Chen, G. F.; Yang, X.; Wang, H. Ammonia synthesis under ambient conditions: selective electroreduction of dinitrogen to ammonia on black phosphorus nanosheets. *Angew. Chem.* **2019**, 131 (9), 2638-2642, DOI 10.1002/ange.201813174.
- (26) Zhang, X.; Wu, T.; Wang, H.; Zhao, R.; Chen, H.; Wang, T.; Wei, P.; Luo, Y.; Zhang, Y.; Sun, X. Boron Nanosheet: an elemental two-dimensional (2D) material for ambient electrocatalytic N₂-to-NH₃ fixation in neutral media. *ACS Catal.* **2019**, 9, 4609-4615, DOI 10.1021/acscatal.8b05134.
- (27) Fan, Q.; Choi, C.; Yan, C.; Liu, Y.; Qiu, J.; Hong, S.; Jung, Y.; Sun, Z. High-yield production of few-layer boron nanosheets for efficient electrocatalytic N₂ reduction. *Chem. Commun.* **2019**, 55 (29), 4246-4249, DOI 10.1039/C9CC00985J.
- (28) Endoh, E.; Leland, J. K.; Bard, A. J. Heterogeneous photoreduction of nitrogen to ammonia on tungsten oxide. *J. Phys. Chem.* **1986**, 90 (23), 6223-6226, DOI 10.1021/j100281a031.
- (29) Zhang, N.; Jalil, A.; Wu, D.; Chen, S.; Liu, Y.; Gao, C.; Ye, W.; Qi, Z.; Ju, H.; Wang, C. Refining defect states in W₁₈O₄₉ by Mo doping: a strategy for tuning N₂ activation towards solar-driven nitrogen fixation. *J. Am. Chem. Soc.* **2018**, 140 (30), 9434-9443, DOI 10.1021/jacs.8b02076.
- (30) Sun, Z.; Huo, R.; Choi, C.; Hong, S.; Wu, T.-S.; Qiu, J.; Yan, C.; Han, Z.; Liu, Y.; Soo, Y.-L. Oxygen vacancy enables electrochemical N₂ fixation over WO₃ with tailored structure. *Nano Energy*. **2019**, 62, 869-875, DOI 10.1016/j.nanoen.2019.06.019.
- (31) Guo, C.; Yin, S.; Yan, M.; Kobayashi, M.; Kakihana, M.; Sato, T. Morphology-controlled synthesis of W₁₈O₄₉ nanostructures and their near-infrared absorption properties. *Inorg. Chem.* **2012**, 51(8), 4763-4771, DOI 10.1021/ic300049j.
- (32) Viswanathan, K.; Brandt, K.; Salje, E. Crystal structure and charge carrier concentration of W₁₈O₄₉. *J. Solid State Chem.* **1981**, 36 (1), 45-51, DOI 10.1016/0022-4596(81)90190-0.
- (33) Tao, H. C.; Sun, ; Back, S.; Han, Z. S.; Zhu, Q. G.; Robertson, A. W.; Ma, T.; Fan, Q.; Han, B. X.; Jung Y.; Sun, Z. Y. Doping palladium with tellurium for the highly selective electrocatalytic reduction of aqueous CO₂ to CO. *Chem. Sci.* **2018**, 9, 483-487, DOI 10.1039/C7SC03018E.
- (34) Cheng, H.; Ding, L. X.; Chen, G. F.; Zhang, L.; Xue, J.; Wang, H. Molybdenum carbide nanodots enable efficient electrocatalytic nitrogen fixation under ambient conditions. *Adv. Mater.* **2018**, 30 (46), 1803694, DOI 10.1002/adma.201803694.
- (35) Xie, S. J.; Bia, Z. J.; Chen, Y. B.; He, Xi. L.; Guo, X. X.; Gao, X. D.; Li, X. M. Electrodeposited Mo-doped WO₃ film with large optical modulation and high areal capacitance toward electrochromic energy-storage applications. *Appl. Surf. Sci.*, **2018**, 459, 774-781, DOI 10.1016/j.apsusc.2018.08.045.
- (36) Watt, G. W.; Chrisp, J. D. Spectrophotometric method for determination of hydrazine. *Anal. Chem.* **1952**, 24 (12), 2006-2008, DOI 10.1021/ac60072a044.